ACS Sustainable Chemistry & Engineering

pubs.acs.org/journal/ascecg

Research Article

Electrochemical Struvite Precipitation Enhanced by an Amelogenin Peptide for Nutrient Recovery

Ivy Wu, Jacob D. Hostert,[§] Geeta Verma,[§] Mei-Chen Kuo, Julie N. Renner,* and Andrew M. Herring*

Cite This: *ACS Sustainable Chem. Eng.* 2022, 10, 14322−14329

Read Online

ACCESS | Metrics & More | Article Recommendations | Supporting Information

ABSTRACT: Precipitation of struvite ($MgNH_4PO_4{\cdot}6H_2O$) from wastewater is a promising method for recycling phosphorous, which results in a slow-release fertilizer and improves wastewater treatment costs. While chemical struvite precipitation is commercialized, electrochemical precipitation can improve the process from an energy and materials standpoint. However, new methods are needed to increase electrochemical recovery at pH values near typical wastewater conditions (6−9). Here, a surface-bound amelogenin peptide was explored in a model electrochemical system to control struvite growth at neutral pH. Molecular dynamics simulations indicated that the peptide enables favorable Mg^{2+} conformations, which facilitate struvite crystallization. Chronoamperometric studies conducted with a range of immobilized peptides in synthetic wastewater at pH 7.1 produced precipitates characterized as struvite. Peptides loaded onto a gold mesh at a concentration of 19 $\mu g\ mL^{-1}$ led to a 21% increase in struvite precipitation. Longer crystals formed in the presence of surface-bound peptide compared to when no peptide was present, showing that dendritic crystal growth can be achieved at neutral pH. The peptide does not appear to bind to struvite, maintaining struvite purity. Our findings show the viability of electrochemical struvite precipitation for relevant wastewater pH values and highlights how peptides can modulate crystal growth.

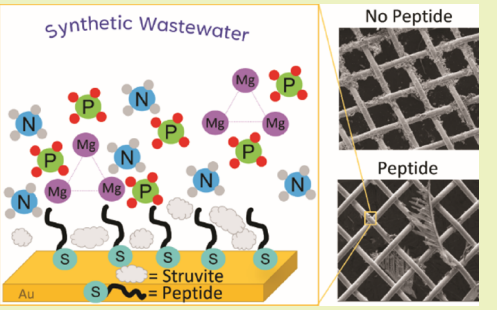

KEYWORDS: *P recycling, struvite, crystal growth, wastewater, electrochemical engineering, amelogenin peptide*

INTRODUCTION

Struvite ($MgNH_4PO_4{\cdot}6H_2O$) recovery from wastewater is one solution to the need for recyclable phosphorous (P) sources, especially since mined P is inherently unsustainable.[1,2] Dedicated struvite recovery units help eliminate unwanted spontaneous sludge formation in pipes. Furthermore, effluents containing high concentrations of P and nitrogen (N) have led to eutrophication in receiving waters.[3] Struvite is recognized as a sustainable slow-release fertilizer,[4−7] and companies have successfully produced struvite fertilizer via chemical precipitation. These dedicated units require expensive magnesium (Mg) salts and pH additives. Recently, interest in electrochemically precipitated struvite has grown, simplifying the process and potentially reducing costs, while maintaining the same or greater crop yields as conventional materials.[8−10] However, further improvements are needed for high electrochemical struvite yields at neutral pH.

In electrochemical struvite precipitation, a sacrificial Mg anode provides Mg^{2+}, eliminating the need for Mg salts. Desirably, the only input to struvite precipitation is Mg since over half the mass of Mg salts is essentially inert to the process. Electrons applied under current or potential control oxidize the Mg anode (eq 1) and produce hydrogen, a valuable energy carrier,[9,11−13] at the cathode (eq 2):

$$Mg_{(s)} \rightarrow Mg^{2+} + 2e^- \quad (1)$$

$$2H_2O_{(l)} + 2e^- \rightarrow 2OH^- + H_{2(g)} \quad (2)$$

Currently, high struvite recovery requires an elevated pH between 8.5 and 10, where struvite is least soluble.[14] Hug and Udert reported electrochemically precipitated struvite from urine, removing 59−84% of P with an initial pH of 8.9 ± 0.1.[15] Others have demonstrated more than 90% P removal and 80−90% N removal via electrochemical processes at elevated pH and are summarized elsewhere.[14] However, typical wastewater pH ranges from 6−9. Methods to increase struvite recovery near neutral pH are needed to expand the technology to different wastewater sources, eliminate excessive additives, and avoid co-precipitation of salts, which reduce struvite purity above pH 8.[16] The utilization of peptides is one potential method to control struvite precipitation at pH < 9, as minerals in nature are precipitated near neutral pH and can be mediated by peptides. Amelogenins are a class of peptides which control the mineralization of tooth enamel. Dogan et al. developed an amelogenin peptide with an affinity toward Ca^{2+} and PO_4^{3-} for

Received: August 8, 2022
Revised: October 4, 2022
Published: October 18, 2022

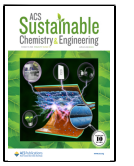

https://doi.org/10.1021/acssuschemeng.2c04691
ACS Sustainable Chem. Eng. 2022, 10, 14322−14329

dental lesion remineralization.[17,18] Mg and Ca are divalent, so this peptide is promising to facilitate struvite growth. The smaller ionic radius of Mg^{2+} (r = 79 pm) compared to Ca^{2+} (r = 100 pm) suggests peptide incorporation into the struvite precipitate may not occur as the mechanism will likely differ between ions.

We previously conducted a small volume study showing this amelogenin peptide increases struvite yield in solution.[19] Here, we capped the peptide with cysteine (C-shADP5) to attach it to a gold (Au) substrate and investigated its ability to affect struvite formation when surface-bound. Au mesh was chosen as a model substrate to demonstrate that cysteine-capped peptides could be effectively immobilized to a surface, allowing for decreased peptide consumption and greater struvite purity compared to peptide free in solution. We probed C-shADP5 peptide binding to struvite via quartz crystal microbalance (QCM) studies, then performed molecular dynamics (MD) simulations to investigate how the presence of the C-shADP5 peptide affects ions in solution. We investigated the surface-bound peptide's utility for electrochemical struvite generation in synthetic wastewater at pH 7.1. Precipitate morphology was studied as a function of peptide surface loading and struvite recovery calculated. Overall, the goal was to investigate the utility of engineered biomolecules to enhance electrochemical struvite precipitation at neutral pH.

EXPERIMENTAL MATERIALS AND METHODS

Materials. Mg ribbon (99.8%) and stainless steel (316) were obtained from Alpha Chemicals and ATI Flat Rolled Products, respectively. Ammonium dihydrogen phosphate and ammonium hydroxide (ACS grade) were obtained from Sigma-Aldrich and Fisher Scientific, respectively. 18.2 MΩ deionized (DI) water was generated from a MilliQ water filtration system. Au mesh (20 mm × 20 mm, 65% wires/inch 99.9% purity) was obtained from Goodfellow Cambridge Ltd. Peptides were obtained from GenScript in lyophilized form with ≥95% purity.

Peptide Design. Peptides were designed based on our previous study.[19] To facilitate Au binding, a cysteine residue was placed on the N-terminus of the peptide followed by three glycine residues as spacers. The final sequence of the peptide is: CGGGSYENSH-QAINVDRT and its primary structure shown in Figure S1. The N and C termini were acetylated and amidated, respectively, to improve the stability of the peptide.

QCM with Dissipation Monitoring. QCM with dissipation monitoring (QCM-D, Q-Sense Explorer, Q-Soft integrated software, Biolin Scientific) was used to investigate the adsorption of struvite to surface-bound peptide. Frequency shifts and dissipation changes were monitored with time. Au-coated crystal sensors (QSX 301, 5 MHz, Biolin Scientific), module cleaning, and other details are found in our previous work and described in the Supplemental Information.[20] Generally, experiments were conducted at 18 °C at 150 μL/min. Struvite crystals were prepared according to our previous work.[19] A 1.25 mg/mL struvite slurry was mixed by adding struvite crystals to the appropriate amount of water and continuously mixed via a stir bar. Peptide was introduced to the system at 10 μg/mL in DI water prior to the introduction of struvite slurry. Struvite binding was examined on bare Au sensors and QCM-D data were analyzed using the seventh overtone (35 MHz) by QSense Dfind software (Biolin scientific).

MD. MD simulations of ions in water with and without peptide were performed using GROMACS package.[21,22] In all simulations, system energy was first minimized using the steepest descent algorithm to remove overlap between atoms. The systems were equilibrated for 10 ns with an integration time step of 2 fs, sufficient for equilibration and ion clustering. The simulations continued for another 50 ns production run under these conditions. Trajectories were saved every 10 ps and visualized in visual MD (VMD) package.[23] Additional details including force field and water models are described in the Supplemental Information.

Preparing Peptide-Functionalized Mesh Samples. Au mesh was cleaned by submerging in Piranha solution for 8 h followed by thoroughly rinsing with DI water. Peptide solutions of varying concentrations were created by pipetting a concentrated peptide solution into a jar containing Au mesh in desired volumes, immediately followed by DI water dilution to achieve final peptide concentrations of 5−25 μg mL^{-1}. The solutions were covered and slowly stirred overnight. The peptide-loaded Au mesh was then rinsed with DI water and dried under nitrogen. For simplicity, the varying peptide loadings on Au are labeled by the peptide concentration during incubation.

Electrochemical Experiments. 120 mM ammonium dihydrogen phosphate was mixed fresh for each test, and pH was adjusted to 7.1 with ammonium hydroxide. 30 mL of this solution was added to a 3D printed reactor containing a stir bar and peptide-loaded mesh (Figure S2). Mg (exposed area 2.4 cm^2), 316 stainless steel, and an Ag/AgCl reference electrode were connected to a Biologic VSP-300 potentiostat. Linear sweep voltammograms were recorded from −1.27 to 1 V at 10 mV/s, which is fast enough to avoid influence of an insulating layer forming on Mg.[24] For struvite precipitation experiments, −0.5 V was applied for 3 h and the chronoamperometric response was measured while constantly stirred at 300 rpm via a stir bar.

Precipitate Collection. The solution was vacuum filtered through 1.5 μm Whatman 934-AH glass microfiber filters. Precipitates collected on the filter, walls of the reactor, Mg, and Au mesh were dried at 40 °C for 8 h before mass was recorded. The faradaic efficiency (FE) was calculated from Faraday's law, described in the Supplemental Information.

Precipitate Characterization. Precipitates were analyzed by Fourier transform infrared spectroscopy (FTIR) on a Thermo Scientific Nicolet iN10 infrared microscope with a germanium attenuated total reflectance tip with 256 scans in the spectra range of 675−4000 cm^{-1} with a resolution of 4 cm^{-1} for all scans. X-ray diffraction (XRD) on a Siemens D500 diffractometer was performed from 10 to 40° ($2\theta/\theta$) at 2 °/min at 30 kV and 15 mA using Cu Ka (1.541874 A) followed by peak identification and analysis using Match! (Crystal Impact GbR) and Jade 9 (MDI Inc.) software. Peak intensities were normalized to the 111 plane. Scanning electron microscopy (SEM) and energy dispersive X-ray (EDX) spectroscopy were performed using a FEI Quanta 600i Environmental SEM.

Statistical Analysis. Minitab was used to calculate 95% confidence interval error bars and run analysis of variance (ANOVA) and Tukey's *post hoc* test with α = 0.05 to determine statistical significance between peptide-functionalized Au.

RESULTS AND DISCUSSION

The shADP5 peptide was shown previously to increase the formation constant and yield parameter of struvite, but binding to struvite crystals was not explored.[19] Here, we modified the peptide by capping it with a cysteine residue, C-shADP5. This peptide was then immobilized onto Au mesh and chosen due to its reliable thiol binding mechanism. Binding of the peptide with struvite was then investigated.

Peptide Binding. QCM-D was used to examine the binding of struvite to the Au-bound C-shADP5 peptide. First, we examined how the struvite slurry bound to a bare Au sensor, Figure 1a. Introducing struvite slurry decreased the frequency, indicating mass addition to the sensor surface. For 20 min, the frequency continuously dropped; the maximum frequency shift was ∼35 Hz. Upon changing the solution to DI water, the frequency rapidly returned to the baseline level, indicating all adsorbed struvite rinsed off. Comparing this bare Au result to a peptide-modified sensor, we can determine if the C-shADP5 peptide binds struvite.

https://doi.org/10.1021/acssuschemeng.2c04691
ACS Sustainable Chem. Eng. 2022, 10, 14322−14329

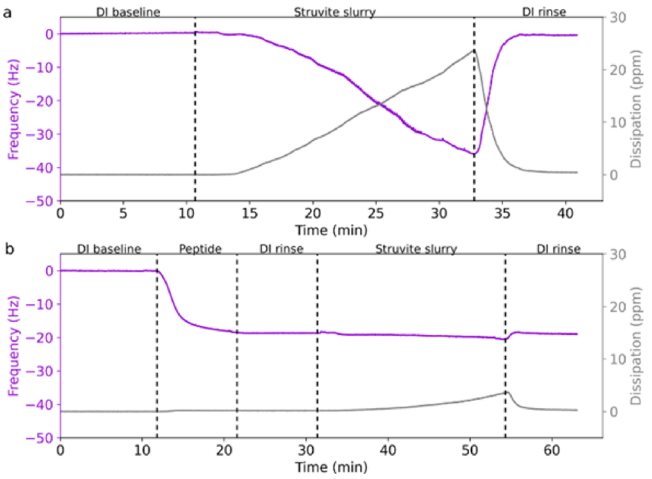

Figure 1. QCM-D frequency and dissipation shifts as a function of time for (a) bare gold sensor and (b) C-shADP5 peptide-modified sensor. Seventh overtone is shown. Frequency is shown in purple, and dissipation is shown in gray. Dashed vertical lines correspond to when the solution is changed, with the solution label above the plot.

In Figure 1b, we first adsorb the peptide to the sensor surface before introducing a struvite slurry, where the frequency shift reaches ∼18 Hz and did not change upon a DI water rinse, indicating the peptide formed a stable layer on the Au surface. When the peptide-functionalized Au surface was exposed to a struvite slurry, a maximum frequency shift of ∼2.5 Hz was observed (lower than the bare Au surface), which once again rinses off when the system was changed to DI water. These results show that the peptide does not have a high affinity for solid struvite in solution. We would not expect bound struvite to rinse off readily (or, would expect the crystals to rinse off slowly through dissolution) when the system is changed to DI water. Interestingly, the peptide seems to be somewhat antifouling toward struvite. The bare Au surface allows copious amounts of nonspecific struvite adsorption while the peptide-modified surface allows minimal struvite adsorption. This property is likely to be useful in struvite precipitation as the surface will not become fouled and require frequent cleaning. Altogether, this peptide-system is beneficial for nutrient recovery, as the immobilized peptide is not consumed and therefore can be constantly utilized giving enhanced and directed high purity struvite.

MD Simulation. Previous studies indicate that certain peptide conformations induce nucleation by forming a crystal matching template, where the peptide encourages the arrangement of ions in a geometry favorable for crystal formation.[25,26] In this work, we adopted a similar methodology to investigate struvite formation. First, a structural analysis of the struvite unit cell was performed. We found that Mg^{2+} and NH_4^+ formed equilateral triangles whereas PO_4^{3-} forms an isosceles triangle. Next, we used MD simulation to see if matching pattern molecular geometries could be detected in the presence of the peptide and compare those geometries to simulations without the peptide. Snapshots of the initial and final configurations, and the total energy and temperature as a function of simulation time, are displayed in Figures S3 and S4, respectively.

The MD trajectories were visualized using VMD to investigate local supersaturations that may lower the activation energy for nucleation and drive mineral growth. Figure 2a shows a snapshot of such local clustering near the peptide solved in water.

Careful examination of the trajectories found that Mg^{2+} equilateral triangles are occasionally formed around the peptide surface like in the struvite crystal as shown in Figure 2b, but do not form without the peptide in water. The full videos of simulation results are displayed in Video S1 and S2. We note that the formation of Mg^{2+} equilateral triangles is transient, where formation and disbandment occur throughout the course of the simulations, perhaps due to peptide conformation changes and the corresponding change in intermolecular interactions. We hypothesize this transient clustering causes increased local supersaturation of Mg^{2+} in favorable orientations, which will increase struvite yields in the presence of peptide and alter morphology. When looking at NH_4^+ and PO_4^{3-} ions, no such matching geometries found in the unit cell are formed.

To further investigate and illustrate the differences in Mg^{2+} arrangement, the radial distribution function (RDF) was used to find the distance between Mg^{2+} ions. A comparison of RDFs of Mg^{2+} in the clusters in the presence of the peptide and without the peptide is shown in Figure 3. Three independent simulation runs are shown.

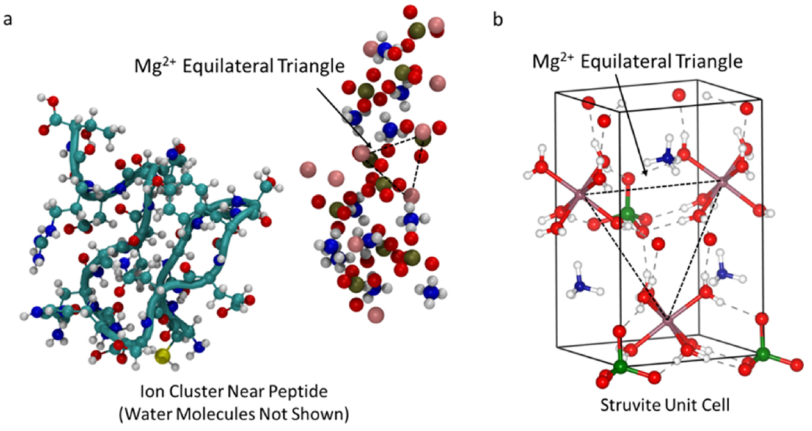

Figure 2. MD snapshots showing the (a) ion cluster near the peptide (teal ribbon) with (b) the struvite crystal unit cell. Representative Mg^{2+} triangles (black dashed lines) are shown to compare the atomic arrangement. Mg atoms are shown in pink, P is shown in green, and blue, red, and white correspond to N, O, and H atoms.

https://doi.org/10.1021/acssuschemeng.2c04691
ACS Sustainable Chem. Eng. 2022, 10, 14322−14329

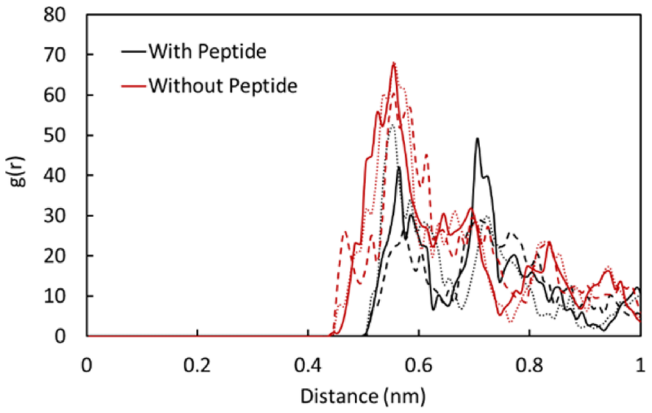

Figure 3. RDF between Mg^{+2} ions in the clusters formed in water with (*black*) and without (*red*) the peptide. Three independent runs are shown using solid, dotted, and dashed lines.

Clearly, the presence of peptide in water shifts peak locations, indicating that the transient atomic arrangement of Mg^{2+} ions is different compared to the case without the peptide. The first peak starts near 0.45 nm without the peptide and shifts to around 0.5 nm in the presence of the peptide. The distance of Mg^{2+} ions in struvite is around 0.69 nm. It seems that intermolecular interactions with peptide in certain conformations shift the ions further apart into desired ionic arrangements. The observed variability in the runs with peptide may be due to constantly changing conformation of peptides near the cluster that creates more random ion arrangements.

In-Situ Struvite Studies. With these promising simulation results, experimental studies of struvite formation in the presence of peptide were conducted. Peptides were immobilized on a model substrate, Au mesh. Synthetic wastewater with sufficient solution conductivity (120 mM ammonium dihydrogen phosphate, 10 mS/cm) was used to gain a clear understanding of peptide influence on precipitates without convolution from foreign ions or high solution resistance. A 3D printed conical reactor, Figure S2, was designed to facilitate diffusion control. The peptide-functionalized Au mesh was placed 1 cm away from the electrode to ensure that it was electrically disconnected. Linear sweep voltammograms are shown in Figure 4.

It is evident from Figure 4 that the peptide-functionalized mesh affects the local ionic concentration and therefore the electrochemistry at the Mg electrode surface. While no monotonic trend among peptide loadings is evident, the presence of the surface-bound peptide reduces the onset potential by roughly 400 mV compared to no peptide on the mesh. The Tafel slopes (Figure S6) were also reduced (from 705 to ca. 405 mV dec^{-1}) in the presence of the immobilized peptide. The similarity in Tafel slopes among all peptide-containing mesh may account for the nonmonotonic trend in linear sweep voltammetry. These results are consistent with our simulations, which showed ion clustering near the peptide may facilitate struvite formation. Struvite formation near the mesh would consume ions, enhancing diffusion away from the Mg electrode, increase the available surface area, and lower the onset potential.

When the reaction was carried out in the batch reactor (Figure S2), white solids were observed to form on the Mg anode and in solution throughout the course of the 3 h chronoamperometry. Figure 5 shows FTIR results and the molar ratio of elements detected by EDX of these precipitates formed with varying loadings of peptide on Au mesh.

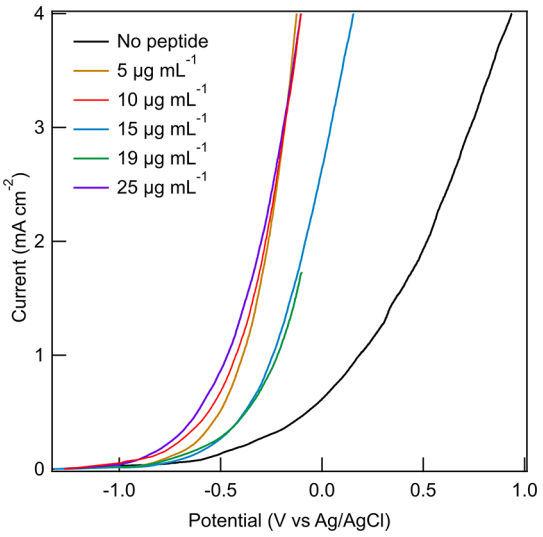

Figure 4. Linear sweep voltammograms swept from −1.27 to 1 V at 10 mV/s of 2.4 cm^2 Mg in 120 mM ammonium dihydrogen phosphate at pH 7.1 and in the presence of Au mesh functionalized with varying peptide concentrations. Black line represents no peptide, while yellow, red, blue, green, and purple lines represent Au incubated with 5, 10, 15, 19, and 25 $\mu g\ mL^{-1}$ peptide, respectively.

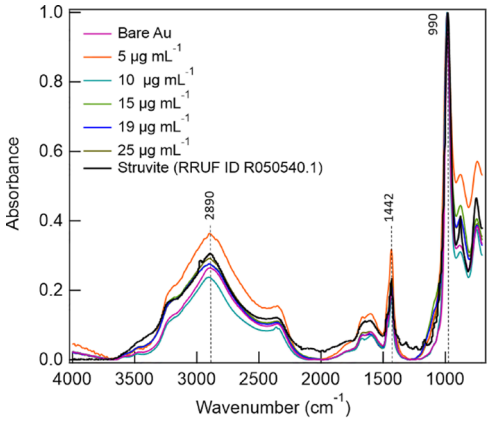

Figure 5. FTIR spectra of precipitates grown during the −0.5 V chronopotentiometric batch reaction in the presence of mesh functionalized with varying concentrations of the peptide. All spectra normalized to 990 cm^{-1}. Pink, orange, teal, green, blue, and gray lines represent Au mesh incubated in 0, 5, 10, 15, 19, and 25 $\mu g\ mL^{-1}$ peptide. Struvite from the RRUFF database is shown in black.

All spectra display similar peaks, matching that of pure struvite. A broad asymmetric band between 2100 and 3600 cm^{-1} is attributed to O−H and N−H stretches. A ν_1 symmetric stretch of NH_4^+ is observed at 2890 cm^{-1}. Absorptions between 1700 and 1600 cm^{-1} are attributed to H−O−H bending of water crystallization. Sharp peaks are observed near 1000 and 1442 cm^{-1}, characteristic of PO_4^{3-} stretch and NH_4^+ bend, respectively.[27−30] Overall, these bands indicate that struvite is the main precipitate.

EDX analysis detected only Mg, O, and P in the precipitates, and their relative molar ratios are displayed in Figure S7. For all peptide loadings, the expected molar ratio of 1:1 Mg:P and 1:4 Mg:O was observed. These results are further evidence that

https://doi.org/10.1021/acssuschemeng.2c04691
ACS Sustainable Chem. Eng. 2022, 10, 14322−14329

the precipitates are struvite as opposed to other magnesium phosphate variations ($Mg_3(PO_4)_2$, $Mg_2(PO_4)(OH)$, and $Mg_3(PO_4)_2{\cdot}8H_2O$). Furthermore, no peptide was detected in the precipitate, as is consistent with our QCM-D data (Figure 1).

To further confirm the identity of the precipitates, XRD was performed and the results are displayed in Figure 6. All spectra were normalized to the 111 index.

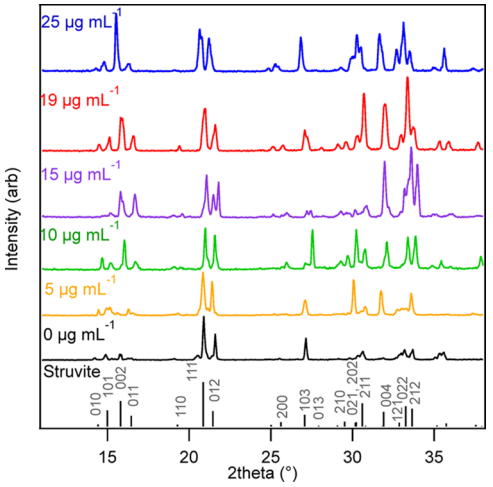

Figure 6. XRD pattern of precipitates grown during the −0.5 V chronopotentiometric batch reaction in the presence of mesh functionalized with varying concentrations of peptide normalized to the 111 index. Gray sticks show struvite reference #9007674 from the Crystallography Open Database. Blue, red, purple, green, yellow, and black lines represent Au incubated in 25, 19, 15, 10, 5, and 0 μg mL^{-1} peptide, respectively.

The 2θ peak locations for all samples match that of the struvite reference,[31] indicating again that struvite is the primary precipitate. The crystallite size calculated from the 111 plane (Figure S8) showed an increasing trend with increasing peptide loadings with the maximum size occurring in samples prepared in 19 and 25 μg mL^{-1} peptide. Similar results were obtained when calculating the crystallite size on the 004 plane. It was important to compare results obtained from the 111 and 004 planes because the highest intensity shifts from the 111 index in samples prepared with peptide concentrations <10 μg mL^{-1} to the 002 and 004 index in samples prepared with peptide concentrations >10 μg mL^{-1}. Changes in the intensity of XRD peaks are attributed to changes in crystal orientation, texture, and shape of the crystalline material.[32] Some studies have reported varying XRD intensities due to greater Mg^{2+} or Ca^{2+} incorporation, but the EDX data (Figure S7) do not support that explanation for our precipitates.[28,33] To probe this result further, SEM images were taken of the precipitates on Au mesh and are shown in Figure 7.

In all cases with the peptide, Figure 7b–f, precipitates displayed a dendritic morphology with a high aspect ratio compared to the coffin-like precipitates formed without the peptide, Figure 7a. This morphology occurs even at the lowest peptide concentration, 5 μg mL^{-1}, Figure 7b. These results are consistent with the mobile peptide, shADP5, which has been reported to induce the formation of dental enamel rods.[18] Without the peptide, polyhedral crystals with well-defined facets were formed (Figure 7a), as is consistent with the literature for struvite formed near neutral pH.[34,35] Figure S9 shows a close-up SEM image of the coffin-like morphology. The low aspect ratio of these precipitates is consistent with the XRD intensity matching that of the reference, with the highest intensity displayed by the 111 index. As peptide concentrations increased, the growth of high aspect ratio, feather-like crystals is consistent with the XRD where, at these high peptide concentrations, the plane of 002 and 004 intensity dominates over the 111 plane (Figure 6). The asymmetry of these planes gives rise to the high aspect ratio morphology. Kirinovic et al. found similar results of struvite XRD intensities changing at different planes, indicating preferential orientation.[30] With different faces dominating and contributing to the higher intensities in the XRD, the peptide clearly affects the struvite growth mechanism and leads to these different morphologies.

Struvite can form various morphologies from orthorhombic to needle-shaped structures depending on pH, concentration, presence of other ions or bacteria, etc.[2,35−37] In particular, high aspect ratio struvite has often been reported to form at pH ≥ 9 and are indicative of faster growth rates.[34,38,39] Shaddel et al. reported a shift in the struvite crystal shape from polyhedral morphology at low supersaturation (1−3) to long dendrites at a supersaturation >5.8.[40] This change in morphology is attributed to a change in the crystal growth mechanism from

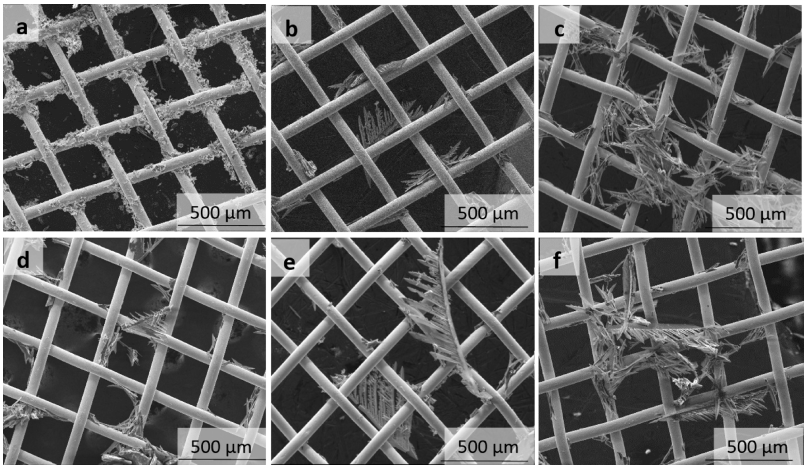

Figure 7. SEM images of solids precipitated on Au mesh prepared in peptide concentrations of (a) 0, (b) 5, (c)10, (d)15, (e)19, and (f) 25 μg mL^{-1} peptide solutions.

https://doi.org/10.1021/acssuschemeng.2c04691
ACS Sustainable Chem. Eng. 2022, 10, 14322−14329

slow, surface-controlled growth to fast, diffusion-controlled growth as the driving force for nucleation (supersaturation) increases. Therefore, the presence of the C-shADP5 peptide alters crystal growth by affecting the local supersaturation, consistent with our simulation results which showed favorable ion clustering near the peptide leading to the different morphologies observed.

Peptides have been shown to affect the growth of crystals via a variety of mechanisms.[41−44] Prywer et al. suggests that the evolution of dendrite-like crystals is primarily affected by the pH rate of change with only minor influence on the pH value.[35] Therefore, the C-shADP5 peptide may be promising for treatment in a wide range of wastewater pH values, and in this study enables a struvite growth mechanism similar to that reported under alkaline conditions but at neutral pH. Prywer et al. also reports that asymmetric ends on the *c*-axis of struvite crystals have different properties that will grow under different mechanisms and form different morphologies, from arrow-heads to X-shapes due to long range dipole−dipole interactions.[35,37,40,45,46] Controlling growth via peptides to different crystal facets could improve the purity of struvite precipitated from wastewater containing multivalent cations such as Ca^{2+} and Fe^{3+}.[47]

Effect of Peptide on Struvite Yield. Peptide-loaded mesh samples incubated in 0−25 μg L^{-1} were explored in a batch reactor. The mass of struvite collected per watt and struvite FE after 3 h chronopotentiometry were calculated and are shown in Figure 8.

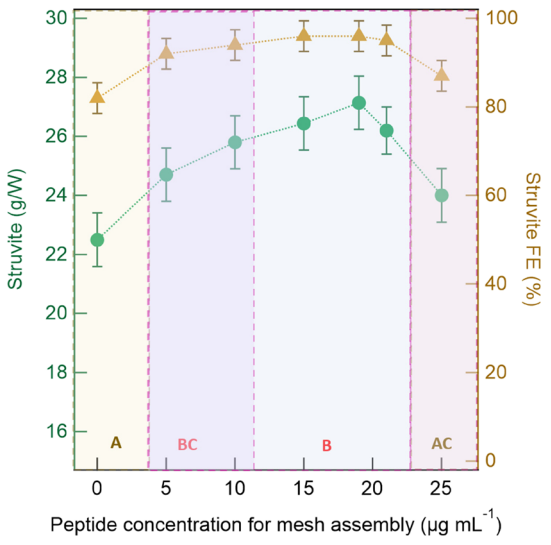

Figure 8. Struvite collected in g/W (green circles) and FE (yellow triangles) with various peptide loadings after 3 h at −0.5 V with a working electrode geometric surface area of 2.4 cm^2. Error bars are 95% confidence intervals. Labeled statistical groupings (A, B, etc) were obtained via ANOVA and Tukey's *post hoc* test—data points that do not share a letter are statistically different at the 95% confidence level.

Interestingly, peptide loadings had a nonmonotonic trend with struvite recovered. The absence of peptide resulted in lower struvite recovery (22.5 g/W) and FE (82%) compared to mesh samples prepared in peptide concentrations of 5−19 μg mL^{-1}. Lower loaded mesh samples prepared in 5−10 μg mL^{-1} peptide solution increased recovery by nearly 15% (25.8 g/W, 94% FE) and increasing peptide concentrations during incubation further to 19 μg mL^{-1} improved recovery to 21% (27.2 g/W, 96% FE). However, samples prepared in higher peptide concentrations decreased struvite recovery to a similar value (24 g/w, 87% FE) as that obtained with no peptide present. Thus, Au mesh samples prepared in any concentration of peptide up to 19 μg mL^{-1} improves struvite recovered, with 15−19 μg mL^{-1} showing the greatest improvement of 18−21%. It is reasonable that a maximum value exists of peptide that can be effectively loaded onto Au mesh, and further increases in the peptide concentration do not allow the peptide to adhere properly to the surface or may impede peptide movement into preferred conformations. Nonpreferred peptide conformations hinder ions moving into positions favorable for struvite formation as shown in our simulations, which was performed with only one peptide and therefore no steric hindrance from additional peptides.

Overall, the C-shADP5 peptide has increased struvite recovery by enabling a similar growth mechanism expected at pH > 9 to occur at pH 7.1. Precipitating struvite 2 pH units lower than the standard will eliminate 400 g of alkaline additive/ton water treated, assuming sodium hydroxide is used. Primary operating costs, simplified to just the electricity and electrode consumption, were calculated following recent literature[12] and described in the Supplemental Information. Promisingly, the primary operating cost for this peptide-mediated process is $0.81/kg struvite, lower than that reported of commercial struvite recovery systems ($5.48/kg struvite).[48] A detailed assessment will be necessitated after moving to realistic wastewater scenarios, but these potential savings are promising and could enable treatment of wastewater with neutral influent pH or after anaerobic digestion.

CONCLUSIONS

The utility of a surface-bound amelogenin peptide, C-shADP5, was explored in a model system as a method to control and increase struvite formation and yield from synthetic wastewater at neutral pH. This peptide was chosen due to its ability to precipitate PO_4^{3+} and Ca^{2+} in tooth enamel applications and was modified for immobilization on Au mesh. QCM-D showed the peptide does not bind to struvite at neutral pH, maintaining struvite purity and avoiding peptide loss. MD simulations showed that the peptide promotes ion clustering and facilitates Mg^{2+} to arrange into favorable orientations for crystallization. Experimental studies in synthetic wastewater at neutral pH found the presence of the immobilized C-shADP5 peptide on Au mesh lowers the onset potential of Mg oxidation by ca. 400 mV, consistent with our simulations suggesting the peptide affects local ionic concentrations and thereby altering the electrochemistry at the Mg surface. Chronoamperometry experiments produced struvite identified via FTIR, EDX, and XRD. Microscopy images showed that struvite formed in the presence of immobilized peptide possessed dendritic instead of polyhedral morphologies typically observed for struvite formed without a peptide present. Dendritic growth indicates local supersaturations and is commonly observed in struvite grown at pH > 9. These results demonstrate how a similar growth mechanism can be achieved at neutral pH by incorporating this peptide-functionalized mesh into the system. Mesh prepared in peptide concentrations up to 19 μg mL^{-1} increased the mass of struvite recovered by 21%, from 22.5 to 27.2 g/W (82 to 96% FE). By enhancing struvite precipitation at neutral pH, these surface-bound peptides increase the viability of electrochemical nutrient recovery without the need for excess chemicals to

https://doi.org/10.1021/acssuschemeng.2c04691
ACS Sustainable Chem. Eng. 2022, 10, 14322−14329

achieve a high pH. Thus, we demonstrated the surface-bound C-shADP5 peptide's utility in enabling wastewater as a sustainable fertilizer source by increasing the type of wastewater that can be used to electrochemically precipitate struvite.

This study utilized a model system with a reliable peptide-substrate binding mechanism (thiol-Au) and high conductivity pure electrolyte to solely investigate peptide−struvite interactions. Now that the bound peptide is shown to enhance struvite precipitation, studies are motivated to move toward realistic conditions. Immobilizing the peptide onto a scalable and inexpensive substrate such as bacteria, which is often already present in wastewater, will improve sustainability. Additionally, design parameters obtained here guides studies on the impact of bound peptides in more complex media.

■ ASSOCIATED CONTENT

Supporting Information

The Supporting Information is available free of charge at https://pubs.acs.org/doi/10.1021/acssuschemeng.2c04691.

Calculations, simulations, peptide structure, reactor schematic, and micrographs (PDF)
Ion clustering in water (AVI)
Ion clustering in the presence of peptide (AVI)

■ AUTHOR INFORMATION

Corresponding Authors

Julie N. Renner − *Department of Chemical and Biomolecular Engineering, Case Western Reserve University, Cleveland, Ohio 44106, United States;* orcid.org/0000-0002-6140-4346; Email: julie.renner@case.edu

Andrew M. Herring − *Department of Chemical and Biological Engineering, Colorado School of Mines, Golden, Colorado 80401, United States;* orcid.org/0000-0001-7318-5999; Email: aherring@mines.edu

Authors

Ivy Wu − *Department of Chemical and Biological Engineering, Colorado School of Mines, Golden, Colorado 80401, United States;* orcid.org/0000-0002-0910-0150

Jacob D. Hostert − *Department of Chemical and Biomolecular Engineering, Case Western Reserve University, Cleveland, Ohio 44106, United States;* orcid.org/0000-0003-3519-7002

Geeta Verma − *Department of Chemical and Biomolecular Engineering, Case Western Reserve University, Cleveland, Ohio 44106, United States*

Mei-Chen Kuo − *Department of Chemical and Biological Engineering, Colorado School of Mines, Golden, Colorado 80401, United States*

Complete contact information is available at: https://pubs.acs.org/10.1021/acssuschemeng.2c04691

Author Contributions

§J.D.H. and G.V. are co-second authors and have contributed equally to this work.

Notes

The authors declare no competing financial interest.

■ ACKNOWLEDGMENTS

We thank NSF (Award #1739473, Award #2133549) and USDA (Award #2018-68011-28691) for financial support. This work used the Extreme Science and Engineering Discovery Environment (XSEDE), which is supported by NSF grant #ACI-1548562. We are grateful to Mr. Kyle Gansemer for 3D printing services.

■ REFERENCES

(1) Desmidt, E.; Ghyselbrecht, K.; Zhang, Y.; Pinoy, L.; Van der Bruggen, B.; Verstraete, W.; Rabaey, K.; Meesschaert, B. Global Phosphorus Scarcity and Full-Scale P-Recovery Techniques: A Review. *Crit. Rev. Environ. Sci. Technol.* **2015**, *45*, 336−384.

(2) Peng, L.; Dai, H.; Wu, Y.; Peng, Y.; Lu, X. A comprehensive review of phosphorus recovery from wastewater by crystallization processes. *Chemosphere* **2018**, *197*, 768−781.

(3) Conley, D. J.; Paerl, H. W.; Howarth, R. W.; Boesch, D. F.; Seitzinger, S. P.; Havens, K. E.; Lancelot, C.; Likens, G. E. Controlling Eutrophication: Nitrogen and Phosphorus. *Science* **2009**, *323*, 1014−1015.

(4) Barak, P.; Stafford, A., Struvite: a recovered and recycled phosphorus fertilizer, in: *Proc. of the 2006 Wisconsin Fertilizer, Aglime & Pest Management Coference*, 2006: 6.

(5) Talboys, P. J.; Heppell, J.; Roose, T.; Healey, J. R.; Jones, D. L.; Withers, P. J. A. Struvite: a slow-release fertiliser for sustainable phosphorus management? *Plant Soil* **2016**, *401*, 109−123.

(6) Omidire, N.; English, L.; Brye, K.; Popp, J.; Greenlee, L., *Struvite: Definition, Benefits, and Potential Application in Arkansas Agriculture*; University of Arkansas, Division of Agriculture Research & Extension. (2020) 7.

(7) Thiessen Martens, J. R.; Entz, M. H.; Schneider, K. D.; Zvomuya, F.; Wilson, H. F. Response of organic grain and forage crops to struvite application in an alkaline soil. *Agron. J.* **2022**, *114*, 795−810.

(8) Omidire, N. S.; Brye, K. R.; English, L.; Popp, J.; Kékedy-Nagy, L.; Greenlee, L.; Roberts, T. L.; Gbur, E. E. Wastewater-recovered struvite evaluation as a fertilizer-phosphorus source for corn in eastern Arkansas. *Agron. J.* **2022**, *114*, 2994−3012.

(9) Kékedy-Nagy, L.; Abolhassani, M.; Perez Bakovic, S. I.; Anari, Z.; Moore, J. P., II; Pollet, B. G.; Greenlee, L. F. Electroless Production of Fertilizer (Struvite) and Hydrogen from Synthetic Agricultural Wastewaters. *J. Am. Chem. Soc.* **2020**, *142*, 18844−18858.

(10) Omidire, N. S.; Brye, K. R.; Roberts, T. L.; Kékedy-Nagy, L.; Greenlee, L.; Gbur, E. E.; Mozzoni, L. A. Evaluation of electrochemically precipitated struvite as a fertilizer-phosphorus source in flood-irrigated rice. *Agron. J.* **2022**, *114*, 739−755.

(11) Hydrogen and Fuel Cell Technologies Office, U.S. Department of Energy, Hydrogen Shot, https://www.energy.gov/eere/fuelcells/hydrogen-shot.

(12) Kékedy-Nagy, L.; English, L.; Anari, Z.; Abolhassani, M.; Pollet, B. G.; Popp, J.; Greenlee, L. F. Electrochemical nutrient removal from natural wastewater sources and its impact on water quality. *Water Res.* **2022**, *210*, No. 118001.

(13) Wu, I.; Teymouri, A.; Park, R.; Greenlee, L. F.; Herring, A. M. Simultaneous Electrochemical Nutrient Recovery and Hydrogen Generation from Model Wastewater Using a Sacrificial Magnesium Anode. *J. Electrochem. Soc.* **2019**, *166*, E576−E583.

(14) Bagastyo, A. Y.; Anggrainy, A. D.; Khoiruddin, K.; Ursada, R.; Warmadewanthi, I.; Wenten, I. G. Electrochemically-driven struvite recovery: Prospect and challenges for the application of magnesium sacrificial anode. *Sep. Purif. Technol.* **2022**, *288*, No. 120653.

(15) Hug, A.; Udert, K. M. Struvite precipitation from urine with electrochemical magnesium dosage. *Water Res.* **2013**, *47*, 289−299.

(16) Hao, X.-D.; Wang, C.-C.; Lan, L.; van Loosdrecht, M. C. M. Struvite formation, analytical methods and effects of pH and Ca2 +. *Water Sci. Technol.* **2008**, *58*, 1687−1692.

(17) Bansal, A.; Shetty, D.; Bindal, R.; Pathak, A. Amelogenin: A novel protein with diverse applications in genetic and molecular profiling. *J. Oral Maxillofac. Pathol.* **2012**, *16*, 395.

(18) Dogan, S.; Fong, H.; Yucesoy, D. T.; Cousin, T.; Gresswell, C.; Dag, S.; Huang, G.; Sarikaya, M. Biomimetic Tooth Repair:

Amelogenin-Derived Peptide Enables in Vitro Remineralization of Human Enamel. *ACS Biomater. Sci. Eng.* **2018**, *4*, 1788−1796.
(19) Hostert, J. D.; Kamlet, O.; Su, Z.; Kane, N. S.; Renner, J. N. Exploring the effect of a peptide additive on struvite formation and morphology: a high-throughput method. *RSC Adv.* **2020**, *10*, 39328−39337.
(20) Su, Z.; Pramounmat, N.; Watson, S. T.; Renner, J. N. Engineered interaction between short elastin-like peptides and perfluorinated sulfonic-acid ionomer. *Soft Matter* **2018**, *14*, 3528−3535.
(21) Van Der Spoel, D.; Lindahl, E.; Hess, B.; Groenhof, G.; Mark, A. E.; Berendsen, H. J. C. GROMACS: Fast, flexible, and free. *J. Comput. Chem.* **2005**, *26*, 1701−1718.
(22) Towns, J.; Cockerill, T.; Dahan, M.; Foster, I.; Gaither, K.; Grimshaw, A.; Hazlewood, V.; Lathrop, S.; Lifka, D.; Peterson, G. D.; Roskies, R.; Scott, J. R.; Wilkins-Diehr, N. XSEDE: Accelerating Scientific Discovery. *Comput. Sci. Eng.* **2014**, *16*, 62−74.
(23) Humphrey, W.; Dalke, A.; Schulten, K. VMD: Visual molecular dynamics. *J. Mol. Graph.* **1996**, *14*, 33−38.
(24) Kékedy-Nagy, L.; Abolhassani, M.; Greenlee, L. F.; Pollet, B. G. An Electrochemical Study of Ammonium Dihydrogen Phosphate on Mg and Mg Alloy Electrodes. *Electrocatalysis* **2021**, *12*, 251−263.
(25) Sahai, N. Modeling apatite nucleation in the human body and in the geochemical environment. *Am. J. Sci.* **2005**, *305*, 661−672.
(26) Yang, Y.; Cui, Q.; Sahai, N. How Does Bone Sialoprotein Promote the Nucleation of Hydroxyapatite? A Molecular Dynamics Study Using Model Peptides of Different Conformations. *Langmuir* **2010**, *26*, 9848−9859.
(27) Muryanto, S.; Hadi, S.D.; Purwaningtyas, E.F.; Bayuseno, A.P., *Effect of Orthosiphon aristatus leaves extract on the crystallization behavior of struvite (MgNH4PO4.6H2O)*, 201410.
(28) Korchef, A.; Saidou, H.; Amor, M. B. Phosphate recovery through struvite precipitation by CO2 removal: Effect of magnesium, phosphate and ammonium concentrations. *J. Hazard. Mater.* **2011**, *186*, 602−613.
(29) Song, Y.-H.; Qiu, G.-L.; Yuan, P.; Cui, X.-Y.; Peng, J.-F.; Zeng, P.; Duan, L.; Xiang, L.-C.; Qian, F. Nutrients removal and recovery from anaerobically digested swine wastewater by struvite crystallization without chemical additions. *J. Hazard. Mater.* **2011**, *190*, 140−149.
(30) Kirinovic, E.; Leichtfuss, A. R.; Navizaga, C.; Zhang, H.; Schuttlefield Christus, J. D.; Baltrusaitis, J. Spectroscopic and Microscopic Identification of the Reaction Products and Intermediates during the Struvite ($MgNH_4PO_4 \cdot 6H_2O$) Formation from Magnesium Oxide (MgO) and Magnesium Carbonate ($MgCO_3$) Microparticles. *ACS Sustainable Chem. Eng.* **2017**, *5*, 1567−1577.
(31) Ferraris, G.; Fuess, H.; Joswig, W. Neutron diffraction study of MgNH 4PO4*6H2O (struvite) and survey of water molecules donating short hydrogen bonds. *Acta Crystallogr. Sect. B.* **1986**, *42*, 253−258.
(32) Pan, Y.; Zhu, T.; He, Z. Minimizing effects of chloride and calcium towards enhanced nutrient recovery from sidestream centrate in a decoupled electrodialysis driven by solar energy. *J. Cleaner Prod.* **2020**, *263*, No. 121419.
(33) Liu, X.; Wang, J. Impact of calcium on struvite crystallization in the wastewater and its competition with magnesium. *Chem. Eng. J.* **2019**, *378*, No. 122121.
(34) Prywer, J.; Torzewska, A. Bacterially Induced Struvite Growth from Synthetic Urine: Experimental and Theoretical Characterization of Crystal Morphology. *Cryst. Growth Des.* **2009**, *9*, 3538−3543.
(35) Prywer, J.; Torzewska, A.; Płociński, T. Unique surface and internal structure of struvite crystals formed by Proteus mirabilis. *Urol. Res.* **2012**, *40*, 699−707.
(36) Doyle, J. D.; Parsons, S. A. Struvite formation, control and recovery. *Water Res.* **2002**, *36*, 3925−3940.
(37) Manzoor, M. A. P.; Singh, B.; Agrawal, A. K.; Arun, A. B.; Mujeeburahiman, M.; Rekha, P.-D. Morphological and microtomographic study on evolution of struvite in synthetic urine infected with bacteria and investigation of its pathological biomineralization. *PLoS One* **2018**, *13*, No. e0202306.
(38) Borgerding, J. Phosphate Deposits in Digestion Systems. *J. Water Pollut. Control Fed.* **1972**, *44*, 813−819.
(39) Leng, Y.; Soares, A. The mechanisms of struvite biomineralization in municipal wastewater. *Sci. Total Environ.* **2021**, *799*, No. 149261.
(40) Shaddel, S.; Ucar, S.; Andreassen, J.-P.; Østerhus, S. W. Engineering of struvite crystals by regulating supersaturation − Correlation with phosphorus recovery, crystal morphology and process efficiency. *J. Environ. Chem. Eng.* **2019**, *7*, No. 102918.
(41) Farmanesh, S.; Chung, J.; Sosa, R. D.; Kwak, J. H.; Karande, P.; Rimer, J. D. Natural Promoters of Calcium Oxalate Monohydrate Crystallization. *J. Am. Chem. Soc.* **2014**, *136*, 12648−12657.
(42) Yang, L.; Li, Y.; Qian, B.; Hou, B. Polyaspartic acid as a corrosion inhibitor for WE43 magnesium alloy. *J. Magnes. Alloys* **2015**, *3*, 47−51.
(43) Li, H.; Yu, S.-H.; Yao, Q.-Z.; Zhou, G.-T.; Fu, S.-Q. Chemical control of struvite scale by a green inhibitor polyaspartic acid. *RSC Adv.* **2015**, *5*, 91601−91608.
(44) Cantaert, B.; Beniash, E.; Meldrum, F. C. The role of poly(aspartic acid) in the precipitation of calcium phosphate in confinement. *J. Mater. Chem. B* **2013**, *1*, 6586.
(45) Prywer, J.; Torzewska, A. Biomineralization of struvite crystals by Proteus mirabilis from artificial urine and their mesoscopic structure. *Cryst. Res. Technol.* **2010**, *45*, 1283−1289.
(46) Yao, Q.-Z.; Guan, Y.-B.; Zhou, G.-T.; Fu, S.-Q. Witherite nanorods form mesocrystals: a direct experimental examination of a dipole-driven self-assembly model. *Eur. J. Mineral.* **2012**, *24*, 519−526.
(47) Qin, L.; Putnis, C. V.; Wang, L. Facet-Specific Dissolution−Precipitation at Struvite−Water Interfaces. *Cryst. Growth Des.* **2021**, *21*, 4111−4120.
(48) Martín-Hernández, E.; Martín, M.; Ruiz-Mercado, G. J. A geospatial environmental and techno-economic framework for sustainable phosphorus management at livestock facilities. *Resour. Conserv. Recycl.* **2021**, *175*, No. 105843.

https://doi.org/10.1021/acssuschemeng.2c04691
ACS Sustainable Chem. Eng. 2022, 10, 14322−14329